Asian Journal of Chemistry; Vol. 35, No. 10 (2023), 2451-2460

ASIAN JOURNAL OF CHEMISTRY

https://doi.org/10.14233/ajchem.2023.28170

Extraction of Silica from Different Solid Wastes and Its Application as Catalyst Support for Vapour Phase Oxidation of Aromatic Hydrocarbon

DEEPA MEENA[1], ANKIT SHARMA[1,*], KIRAN PARASHAR[1], DEEPTI GOYAL[2], SAKSHI KABRA MALPANI[3] and ASHU RANI[1]

[1]Department of Pure and Applied Chemistry, University of Kota, Kota-324005, India
[2]Department of Applied Chemistry, University School of Vocational Studies & Applied Sciences, Gautam Buddha University, Greater Noida-201308, India
[3]Save the Water™, 8723 NW 11 Street, Plantation, FL 33322, USA

*Corresponding author: E-mail: ankit@uok.ac.in

Received: 20 June 2023; *Accepted*: 10 August 2023; *Published online*: 28 September 2023; AJC-21396

In present study, the research work has been divided into two sections *viz*. Firstly, amorphous silica was extracted from different silica rich agricultural and industrial waste materials (fly ash, perlite and rice husk ash) *via* sol-gel method. The extracted silica (RHA-Si, Perlite-Si, FA-Si) was characterized using BET surface area, FESEM, EDS, XRD, NMR and FTIR techniques. The surface area and particle size of extracted silica was found to be 23.06-255.5 m^2/g and 61-267 nm. Secondly, fly ash silica was used as catalyst support and modified desirably by loading different molybdenum weight percentages *via* acid impregnation method. The presence of MoO_3 on the surface of extracted silica were confirmed by different characterization techniques. The kinetic studies of the FASi/Mo-15 catalyst for the vapour phase oxidation of benzene was also investigated by employing the Mars Van Krevelen model to analyze the reaction mechanism and rate of the process. The vapour phase oxidation reaction follows zero order kinetics, with faster benzene conversion occurring at lower intake concentrations and higher reaction temperatures.

Keywords: Fly ash, Rice husk ash, Perlite, Extracted silica, Vapour phase, Kinetics.

INTRODUCTION

Silica is widely distributed across the earth and constitutes approximately 32% of the entire mass of the Earth's crust [1]. Silica occurs in nature as silica sand, glass, quartz *etc*. in the form of amorphous, gel or crystalline material. Amorphous silica is a highly pure fine particulates with excellent surface area with tremendous potential as catalyst support, fillers, adsorbents, carriers, *etc.* in various fields like pharmaceuticals, paints, cosmetics, organic reactions, fertilizers, *etc*. [2-8]. It has also been utilized as raw material in ceramic industry, strengthening agent in rubber industry, as laxative in toothpastes, flow conditioners in food industries, *etc.* [9-11]. Precipitated silica has been utilized as a filler in production of shoes, tires, general rubber goods [3,12], while it also bind application as desiccant for moisture adsorption in various household as well as electronic goods. Silica used in various chemical applications is produced from silica precursors such as tetramethylorthosilicate (TMOS), tetraethylorthosilicate (TEOS), polyethoxydisiloxane (PEDS), *etc.* [13-16].

Due to the high cost of the energy needed to heat the precursors and the calcination processes, manufacturing sodium silicate is not economical. Various synthetic procedures reported in the literature for silica precipitation are chemical vapour deposition, combustion synthesis, sol-gel, micro-emulsion processing, plasma synthesis, hydrothermal technique, fluidized bed, carbonization, combustion, *etc.* [4,15,17,18]. Amongst, sol-gel process is common, which involves preparation of sol *via* hydrolysis and gel *via* condensation of silica precursors (TEOS, TMOS and PEDS) in the presence of alcohol, water and NH_3 to form silica [14]. For silica synthesis, the sol-gel method has been the most popular choice due to its many advantages, such as the possibility of performing the synthesis at low temperatures and a suitable pH to offer high yield purity. However, the raw materials *viz*. alkoxides being very expensive, hazardous and can cause blindness (with TMOS), therefore,

their commercialization is prohibited [13]. Commercially sodium silicate is fabricated by reaction of silica containing materials like quartz sand with soda ash or caustic soda in a furnace at higher temperature, generally above 1300 ºC [19]. This method is extremely expensive and environmentally hazardous since it consumes a lot of energy and generate a lot of CO_2, wastewater and sodium sulfate. Therefore, modern industry need a simple, energy-efficient and cost-effective approach of extracting silica, which has numerous practical applications.

As a result, it is necessary to shift to some alternate sources of silica that are readily available, economical and environmentally friendly. The potential substrates in this particular field include natural, industrial, and silica-enriched solid wastes, such as rice husk ash (RHA), perlite and fly ash (FA). Rice husk is a waste of rice milling industries, which is directly dumped or burned consequently may lead to chronic ailments and severe environmental pollution. Fly ash is a waste generated by coal burning during power production at thermal power plants that contributes significantly to global environment pollution in the form of solid waste. While perlite is light weight granular material released from explosive volcanic eruptions in the form of expanded volcanic glass, because of its widespread distribution, perlite may have a variety of negative health effects on civilization, including animals and human beings. Thus, researchers need to look into these solid wastes because of the negative impacts they have on the environment and the lack of adequate policies regarding their disposal and conversion to useful products. The potential of these solid wastes have been explored in new areas such as in synthesis of zeolites [20-22], acid & base catalyst [23,24], mesopororus materials [25,26], *etc.*

Molybdenum based catalysts [27-30] finds applications in homogeneous phase and used as an oxidant in catalytic reactions but shows difficulty in catalyst recovery as well as industrial problems, which is related with deposition of the catalyst and corrosion [31,32]. Many scientists have attempted to reduce this drawback by incorporating molybdenum onto a wide variety of solid supports by adopting different methodology *via* impregnation, sol-gel, $MoO_2(acac)_2$ anchoring and thermal spreading [33-35]. Several support materials have been used such as SnO_2 [36], Al_2O_3 [37], SiO_2 [38], ZrO_2 [39], MoV heteropoly acid (HPA) [40], classical supported catalysts [41, 42] and various types of mesoporous silica *i.e.* MCM-41 [43], SBA-15 [44] and have also been used as support materials. In general, support materials have been employed to promote the dispersion, oxidation state, nuclearity and stabilization of MoO_3 fine particles and it also permits to access a large number of catalytically active atoms which was not available to the reactants over MoO_3 species alone. The chosen metal oxide support and factors associated to the preparation processes, the calcination temperature of the sample and Mo surface density, *etc.* are the crucial factors for the relative concentration of the various MoO_3 surface species [45].

The present work reports the extraction of silica from three solid wastes, rice husk ash (RHA), perlite and fly ash (FA) by using an economical, facile and greener approach. Structure, morphology, chemical bonding of extracted silica is discussed based on results obtained from different characterization techniques such as XRD, FESEM, EDS, BET surface area, FTIR and ^{29}Si NMR. Based on findings during this research, the further utilization of extracted silica in various value-added applications like adsorption, catalyst support, fillers, *etc.* can also be recommended. Out of these applications, catalyst support has been done in this work for catalyst synthesis, fly ash silica have been used as a support of MoO_3 catalysts. Wherein investigation have been done for the characterization of silica supported molybdenum oxide catalyst (FASi/Mo) and their catalytic activity in vapour phase oxidation of benzene. The synthesized catalyst was proven to be more effective and recyclable in oxidation reaction. The kinetic analysis of benzene oxidation in the vapour phase using the experimental data was another goal of this work. The relationship between the catalytic activity and structural features of the extracted silica and MoO_3 species has also been addressed.

EXPERIMENTAL

A sample of fly ash was received from Tata Thermal Power Plant (TTPP), Jamshedpur, India. Perlite was supplied by Indica Chemical Industries Pvt. Ltd. (Kotdwar, India), while rice husk was collected from Ranpur, Kota, (India). Benzene as reactant was supplied by Sigma-Aldrich, whereas NaOH pellets, conc. HCl, ammonium molybdate tetrahydrate, $[(NH_4)_6Mo_7O_{24}]$ were supplied by Rankem, India.

Extraction of silica from rice husk ash (RHA), perlite and fly ash (FA): Dissolution-precipitation technique has been employed for silica extraction from all the three samples (FA, RHA and perlite), involving alkali solubilization and acid precipitation. Initially, all the samples were thoroughly rinsed with 1 N HCl to remove dust and other metallic and organic impurities and then successively washed with distilled water for the removal of acidic impurities. After washing, the samples were utilized as a raw material to produce silica by adopting following procedure:

Acid washed FA, RHA and perlite samples were calcined in muffle furnace at 700 ºC for 3 h. These samples were mixed with 15 wt.% NaOH solution at 70 ºC for 4 h to produce a transparent solution of sodium silicate, which was utilized for silica extraction. The obtained Na_2SiO_3 solution was titrated with 1 M HCl at 90 ºC under constant stirring till pH 7. The solution was left for 24 h under constant stirring. The obtained precipitate was centrifuged and the collected white solid portion was washed thoroughly with hot distilled water and later oven dried at 50 ºC for 24 h. Following formula was used to calculate the yield% of extracted silica.

$$\text{Silica extraction yield (\%)} = \frac{\text{Mass of silica precipitated}}{\text{Mass of solid wastes used}} \times 100$$

Catalyst synthesis: Fly ash silica supported molybdenum oxide (FASi/Mo) catalysts was prepared by acid impregnation method. The Fly ash silica (FASi) was calcined in an muffle furnace at 800 ºC for 3 h, then appropriate amount (3 g for 10 wt.%, 4.5 g for 15 wt.% and 6 g for 20 wt.%) of ammonium molybdate was taken in 50 mL beaker and dissolved with

distilled water. The calcined silica (1 g) was added in above solution and the slurry was aged for 24 h at 30 ºC under constant stirring. The impregnated samples were filtered and washed by ethanol and dried at 100 ºC for 24 h. The prepared samples were calcined in muffle furnace at 550 ºC for 6 h. The prepared catalysts with molybdenum oxide loadings of 10, 15 and 20 wt.% denoted as FASi/Mo-10, FASi/Mo-15, FASi/Mo-20, respectively.

Characterizations: The crystalline index and peak identification of extracted silica was done by X-ray powder diffractometer (Rigaku, Ultima IV) using Cu*K*α radiation (λ = 1.54 Å) at 2θ = 5-80º range with the scanning rate of 0.04º/s. The surface morphology, chemical composition and particle size of samples were analyzed by FESEM microscope (Jeol, JEM2100) and FESEM supported EDS analyzer (Oxford elemental analyzer). The FTIR spectrum was recorded on FTIR spectrophotometer (Tensor-27, Bruker, Germany) in the range of 4000-500 cm^{-1}. Surface area and pore size were analyzed by Quantachrome NOVA using 1000e under inert atmosphere at 120 ºC for 2 h. The ^{29}Si NMR of the samples was recorded by sophisticated multinuclear FT NMR spectrometer, (model Bruker Advance Neo 500 Hz).

Catalytic reactions: Vapour phase oxidation of benzene was performed in vapour phase microreactor. A fixed bed reactor consists of main component which consists of stainless steel tube (4.5 cm long × 2.2 cm inner dia. × 2.54 cm outer dia.) positioned with a PID temperature controlling system in a furnace. A thermocouple was used for measuring temperature positioned into the catalytic bed. The FASi/Mo catalyst (5 g) was preheated for 1 h at 400 ºC in the stream of air (50 mL/min). Then after the catalytic bed was packed inside the vertical reactor tube in which 5 g catalyst was sandwiched among two plugs of glass wool. A mixture of reactant (0.4 mL/min benzene) and air (50 mL/min) was firstly pre-heated at the appropriate temperature, mixed and then delivered into the reactor tube through pre mixer and vapourizer. Here, back pressure control valve and the mass flow controller was used for maintaining pressure conditions and a constant flow rate of air. The reaction mixture was collected in gas liquid separator and cooled to room temperature, after passing through the catalyst bed. A gas-liquid separator was used to collect the effluent and cooled down through a water condenser. The final products was analyzed by a gas chromatograph (Agilent 7820 A). The conversion (%) was calculated by using formula:

$$\text{Conversion } (\%) = \frac{100 \times (\text{Initial wt.\%} - \text{Final wt.\%})}{\text{Initial wt.\%}}$$

RESULTS AND DISCUSSION

Characterization of extracted silica: All the samples of extracted silica show the amorphous nature as observed by the absence of sharp defined peaks in XRD patterns (Fig. 1b, 2b and 3b). The broad hump (gibbous) centred at 22-24º is the characteristic of silica (amorphous) [46]. Absence of any peak attributed to metallic impurities or any other metallic salts like NaCl, Na_2SO_4, *etc.* shows the effectiveness of acid washing of samples which is also confirmed by SEM-EDS results. The XRD patterns of extracted silica samples were found similar to that of commercial silica [47].

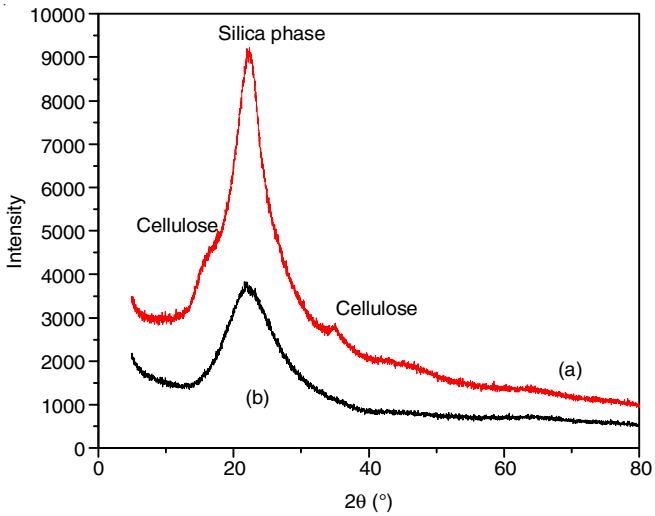

Fig. 1. XRD of (a) rice husk ash (b) RHA-Si

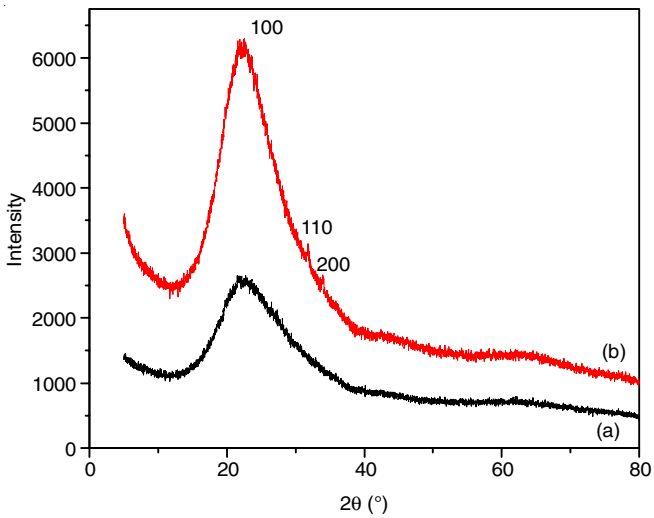

Fig. 2. XRD of (a) perlite (b) perlite-Si

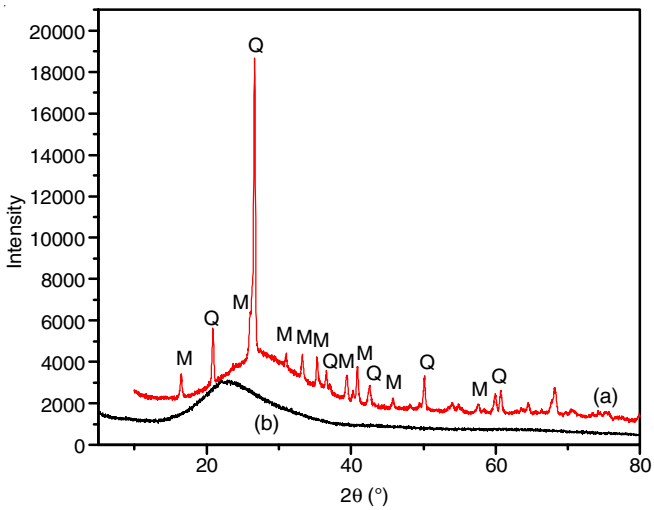

Fig. 3. XRD of (a) fly ash (b) FA-Si

Morphological studies: The FESEM images of the extracted silica are shown in Fig. 4a-i. The FESEM of FA-Si (Fig. 4a-c) revealed that the spherical particles in the size range from 220-267 nm were aggregated together and tends to form a cluster. The FESEM images of rice husk ash-silica (RHA-Si) depicted in Fig. 4d-f exhibit uniform, spherical particles that are somewhat agglomerated, with sizes ranging from 61 to 78 nm. Similarly, FESEM micrographs of perlite-Si (Fig. 4g-i) show same morphology as RHA-Si with different particle size.

The EDS analysis of FA-Si, RHA-Si and perlite-Si are shown in Fig. 5. The presence of silica was confirmed by finding of Si and O in the samples. The absence of any other metallic peak confirms the high purity of all the extracted silica samples.

FTIR studies: The FTIR spectra of FA, RHA and Perlite and FA-Si, RHA-Si and Perlite-Si are shown in Figs. 6-8. The entire spectra shows broad band at 3500-3000 cm^{-1} which is attributed to the stretching vibrations bands of silanol (Si-OH) groups [48-50]. A sharp peak at 1637 cm^{-1} in all silica samples, was due to the bending mode of –OH groups and H_2O molecules [48,49]. A broad band in 1200-1050 cm^{-1} range corresponds to the valence vibrations of Si-O-Si network [48,49,51]. The sharp peaks at 1119 cm^{-1} in FA-Si, 1099 cm^{-1} in RHA-Si and 1101 cm^{-1} in perlite-Si attributed to asymmetric stretching vibration of Si-O-Si and their corresponding symmetrical stretching bands were observed at 801, 806 and 807 cm^{-1}, respectively [48,49,51]. Further, the absence of any other peaks indicates that process of washing was efficient in removal of impurities from the silica.

BET studies: The surface area of FA-Si, RHA-Si and perlite-Si by BET equation was 23.06, 255.5 and 97.55 m^2/g, respectively. The pore size and pore volume of FA-Si, RHA-Si and Perlite-Si were found to be 0.97, 1.91 and 0.71 Å and

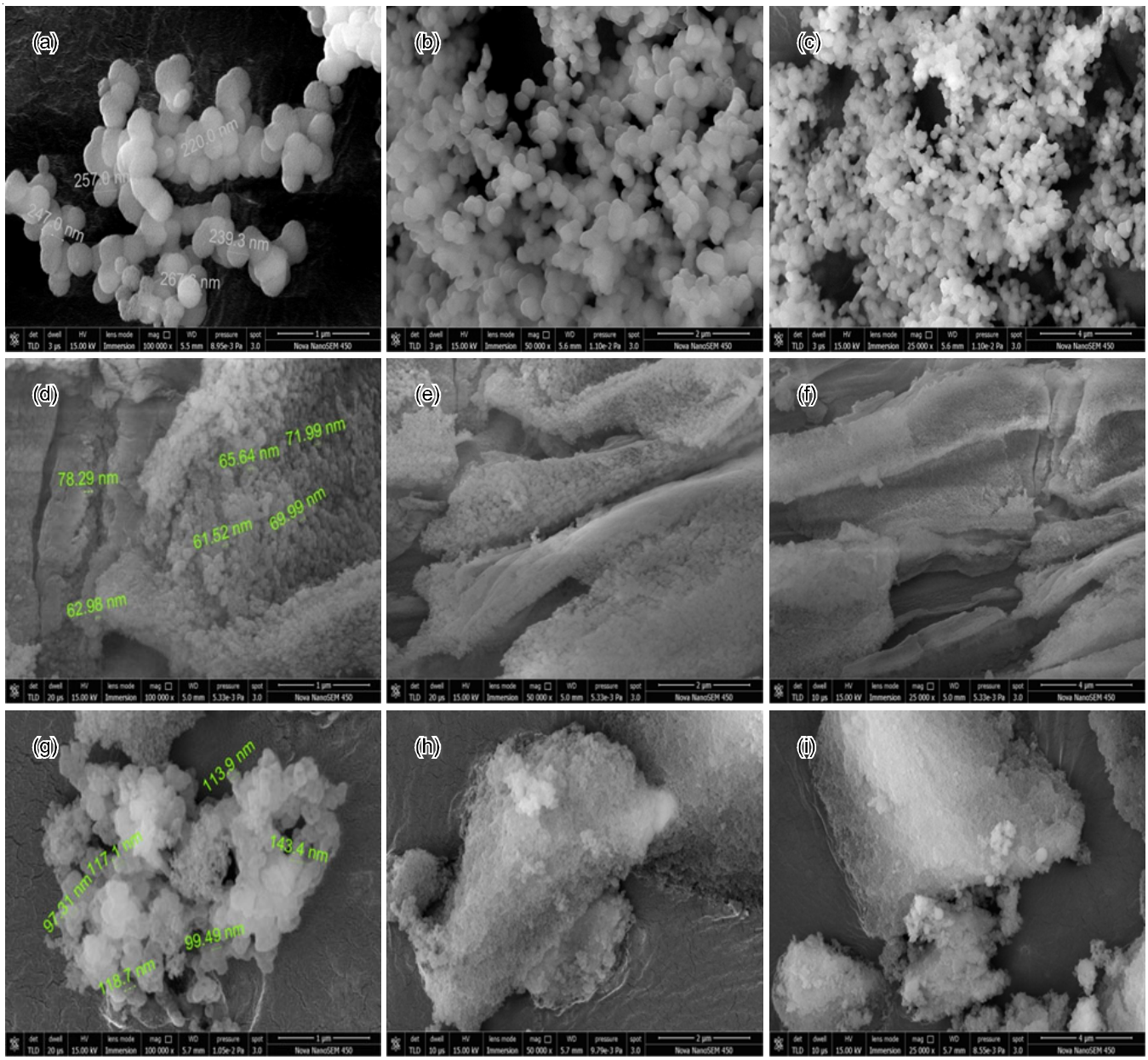

Fig. 4. FE-SEM images of (a,b,c) FA-Si; (d,e,f) RHA-Si and (g,h,i) perlite-Si

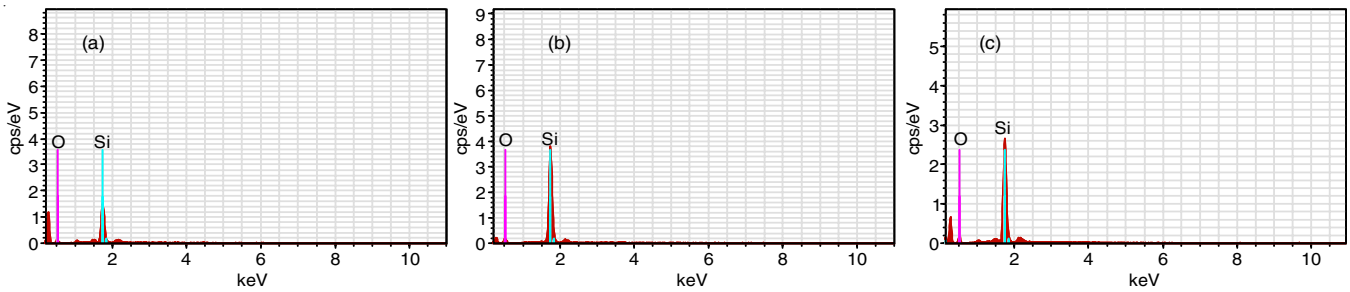

Fig. 5. EDS of (a) FA-Si, (b) RHA-Si and (c) perlite-Si

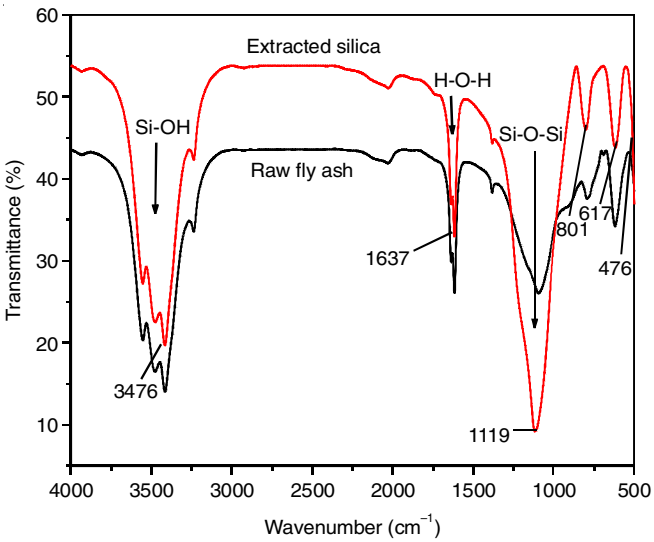

Fig. 6. FTIR spectra of FA and FA-Si

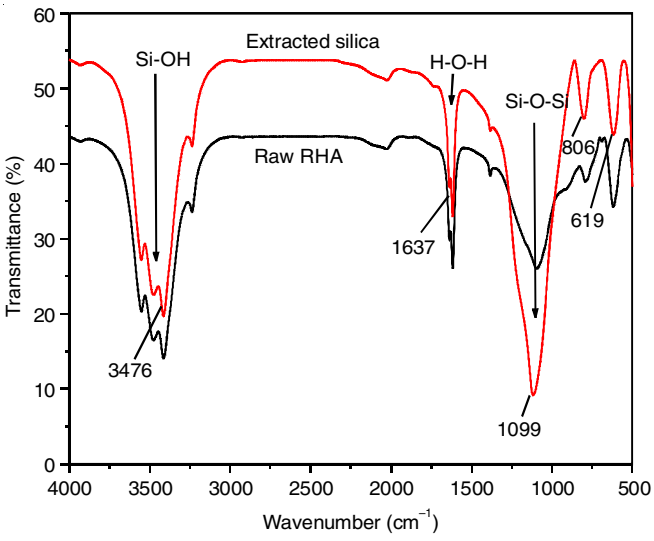

Fig. 7. FTIR spectra of RHA and RHA-Si

0.03, 0.28 and 0.45 cm^3/g, respectively. The textural, structural properties and particle size have been summarized in Table-1.

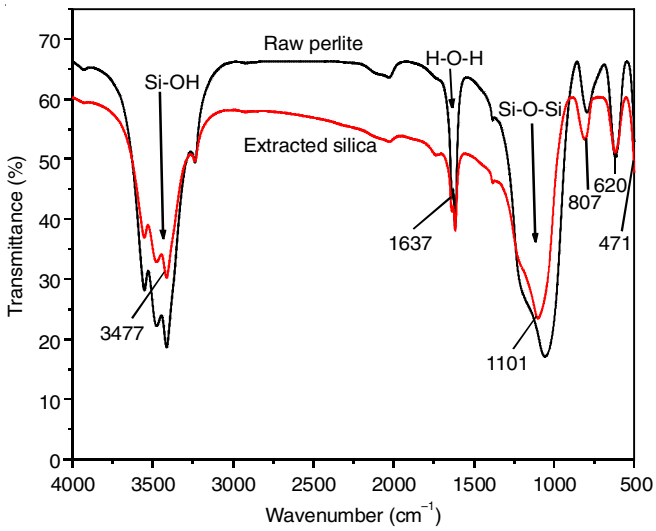

Fig. 8. FTIR spectra of perlite and P-Si

^{29}Si NMR studies: The analysis of ^{29}Si NMR spectra of FA-Si, RHA-Si, perlite-Si shows a band in the range between -91 to -111 ppm, revealing the presence of three types of silanols, *i.e.* germinal silanols (Q^2), single silanols (Q^3) and siloxane groups (Q^4) (Fig. 9), which are the characteristic of amorphous silica [52]. The silica network is designated by the unit Q (denotes to central atom Si) which is linked with oxygen and Al atom by tetrahedral linkage. The peak at -111 ppm indicates the presence of Q^3 and Q^4 units in the extracted silica, which was further confirmed by FTIR spectra. In terms of silica content, it was high in RHA and perlite than FA. Owing to easy availability, FASi was chosen as the catalyst support which was not with perlite and moreover RHA still have residual fuel value to be utilized further.

Characterization of synthesized catalyst: The physico-chemical properties of FASi and different Mo catalysts have been presented in Table-2. The BET surface area of FASi was 23 m^2/g. With the increasing molybdenum content (10 to 20 wt.%), the surface area of synthesized catalysts marginally decreases due to blockage in surface active sites of the support. While wider molybdenum oxide aggregates were aligned towards

TABLE-1
TEXTURAL AND STRUCTURAL PROPERTIES OF FA-Si, RHA-Si AND Perlite-Si

Samples	Silica content (%)	Surface area (m^2/g)	Pore radius (nm)	Pore volume (cm^3/g)	Particle size (nm)
FA-Si	75.91	23.06	0.977	0.0275	220-267
Perlite-Si	80.81	97.55	0.714	0.4532	97-143
RHA-Si	83.76	255.5	1.914	0.2846	61-78

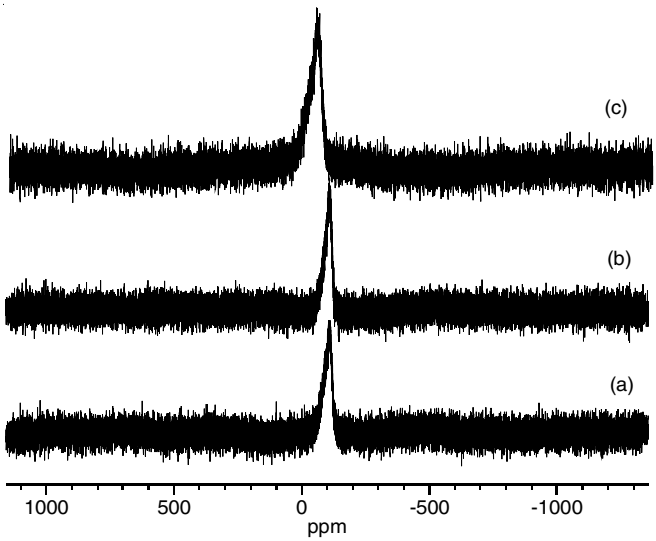

Fig. 9. ^{29}Si NMR spectra of (a) FA-Si (b) perlite-Si and (c) RHA-Si

TABLE-2
PHYSICO-CHEMICAL PROPERTIES OF
FASi AND SYNTHESIZED CATALYSTS

Samples	Silica (wt.%)	Mo content (wt.%)	BET Surface area (m^2/g)
FASi	75.9	0.0	23.0
FASi/Mo-10	76.3	6.8	67.8
FASi/Mo-15	77.1	13.0	45.8
FASi/Mo-20	77.1	19.9	14.2

the external surface of support (FASi), which has blocked the pore entrance being the reason for decrement in surface area values.

Fig. 10 shows the XRD spectra of FASi and FASi/Mo catalyst at different angles ranging from 5 to 80 ºC. FASi displays a broad peak (gibbous) at 2θ = 15-30º (Fig. 10a) attributing to amorphous nature. A typical peak of amorphous silica from 15º to 30º at 2θ was observed for all FASi/Mo catalyst samples (10, 15 and 20 wt.%).The X-ray diffraction (XRD) pattern obtained from the bulk MoO_3 exhibits prominent peaks at

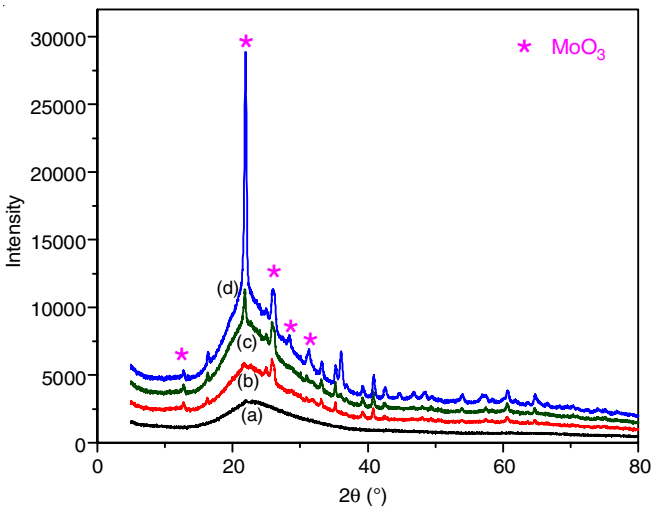

Fig. 10. XRD of (a) FASi, (b) FASi/Mo-10, (c) FASi/Mo-15 and (d) FASi/Mo-20 catalyst

12.9º, 23.4º, 25.8º, 27.4º, and 32.5º. These peaks are indicative of the orthorhombic phase of MoO_3 as previously reported [38]. These same distinctive peaks were also detected in the catalyst under investigation. β-MoO_3 phase was not detected in the XRD spectra of all FASi/Mo catalysts samples because these catalysts were calcined at 550 ºC in which β-MoO_3 phase was unstable [53]. Although the surface area of FASi/Mo catalyst is larger than that of the FASi catalyst, it is important to observe that the FASi support retains its amorphous nature even with increased Mo loading [54], even though MoO_3 is in crystalline form. The catalyst shows the extracted silica hump as well as the crystalline peaks of MoO_3 indicating the well dispersion of MoO_3 on the support (extracted silica).

The absorption bands of the silica support (~ 3400, 1637, 1119 and 801 cm^{-1}) related to the silica framework were retained in all FASi/Mo catalysts samples. As molybdenum loading was done (Fig. 11), the broadness of area 3000-3500 cm^{-1} describes the interaction between molybdate species and FASi. As the Mo loading level were increased the peak at 1119 cm^{-1} due to asymmetric vibration of Si-O-Si was shifted to lower wavenumber attributed to Si-O-Mo stretch in the catalysts. In addition, the appearance of extra peaks in molybdenum catalyst around 794 and 920 cm^{-1} may be assigned to stretching band of oxygen connected with three metal atoms (Mo-O), overlapping of Si-O bending vibration band with Mo=O band.

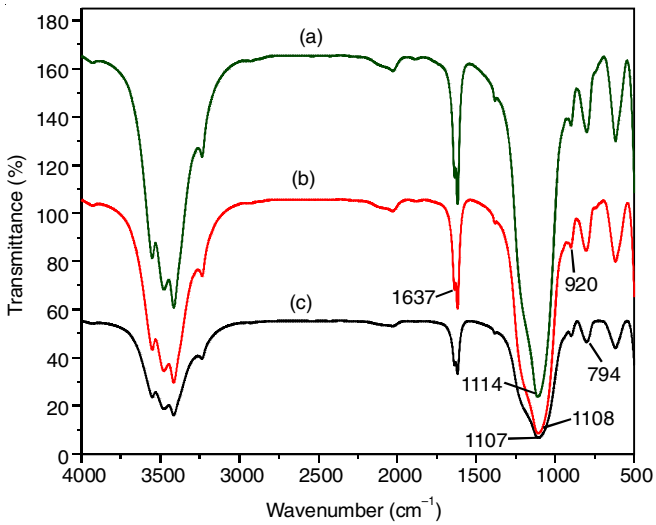

Fig. 11. FTIR spectra of (a) FASi/Mo-10, (b) FASi/Mo-15 and (c) FASi/Mo-20 catalyst

FESEM images (Fig. 12) reveals that FASi (Fig. 12b) has smooth surface without any pores. While FESEM images for FASi/Mo catalyst (Fig. 12c-e) clearly indicates the difference in the surface morphology from that of FASi. The FESEM micrographs of catalyst shows the incorporation of MoO_3, which changes the morphological structure of support surface. The images had proven that the surface area of catalyst decreases with increasing Mo loading as confirmed by BET surface results too.

Catalytic performance results: The catalytic activity of synthesized catalysts were analyzed by oxidation reaction of benzene under vapour phase reaction conditions. Table-3 shows

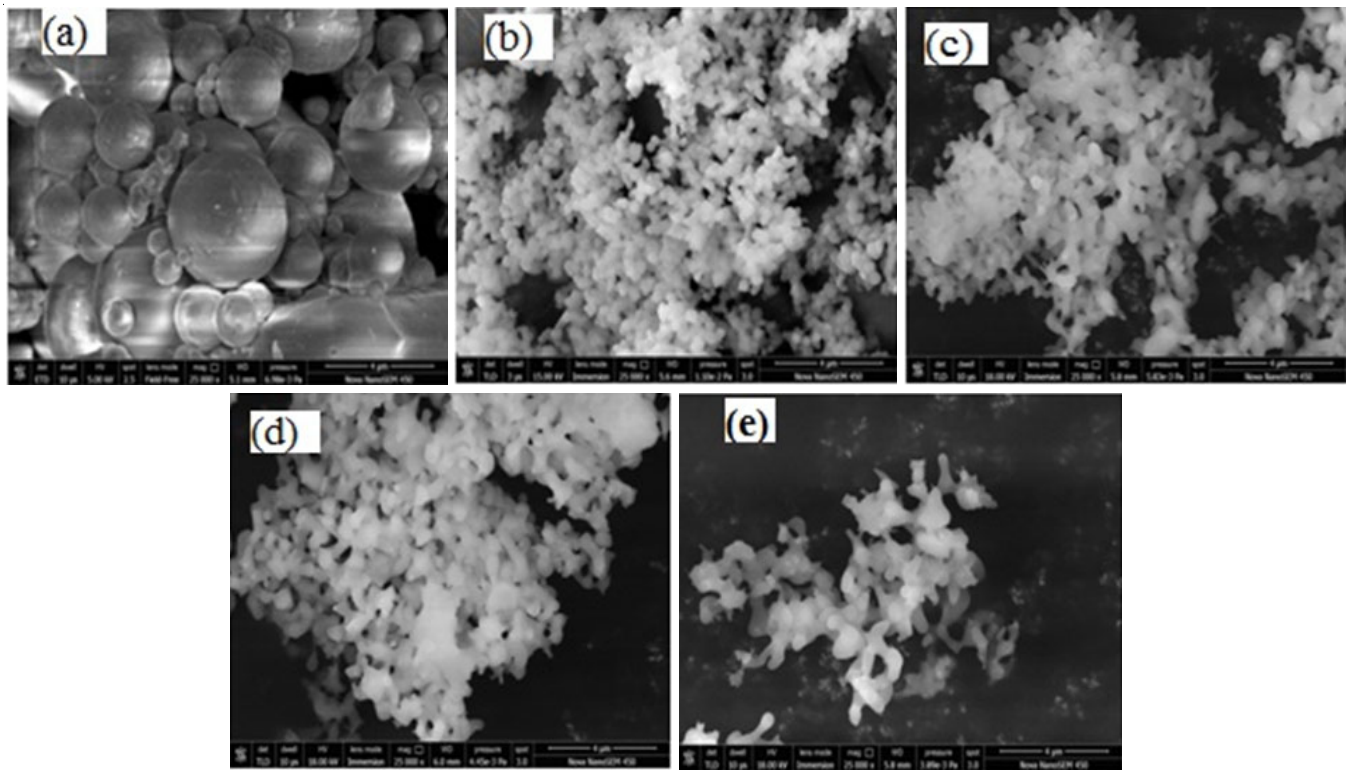

Fig. 12. FE-SEM images of (a) pure fly ash, (b) FASi, (c) FASi/Mo-10,(d) FASi/Mo-15 and (e) FASi/Mo-20 catalyst

TABLE-3
CATALYST PERFORMANCE FOR DIFFERENT CATALYST FOR BENZENE OXIDATION

Samples	Conversion (%)
Without catalyst	Nil
FASi	Nil
FASi/Mo-10	41
FASi/Mo-15	84
FASi/Mo-20	76

that there no reaction occurs in absence of catalyst and FASi alone also do not show any catalytic activity for this oxidation reaction. The conversion was increased from 41 to 84% with increased Mo content from 10 to 15 wt.%. FASi/Mo-15 catalyst shows the maximum conversion due to existence of active monomeric and dimeric molybdate species consisting high amount of Mo-O-support bonds.

In light of above inferences, the vapour phase oxidation of benzene and its kinetics, influence of various reaction parameters like reaction time, temperature, inlet concentration were studied in detail by using FASi/Mo-15 catalyst.

Kinetics of vapour phase oxidation of benzene over FASi/MO-15 catalyst: The oxidation of benzene (**Scheme-I**) was carried out over FASi/Mo-15 catalyst in vapour phase micro reactor by varying parameters like inlet concentration of benzene and temperature. Inside the vertical reactor tube, 5 g of FASi/Mo-15 catalyst was placed for vapour phase oxidation. Before each experiment, the FASi/Mo-15 catalyst was pre-heated at 400 ºC for 1 h under flow of air (50 mL/min). The oxidation reaction was carried out of benzene and flowing air (100 mL/min) passing through pre-mixer heater at different temperature range (623-663 K) and different inlet concentration of reactant.

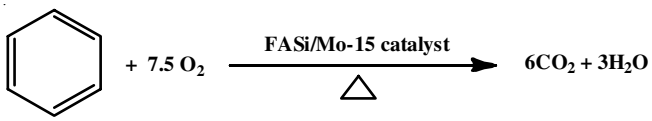

Scheme-I: Reaction scheme for benzene oxidation over FASi/Mo-15 catalyst

Effect of temperature: The influence of temperature (623 to 663 K) on conversion was studied for the oxidation of benzene over FASi/Mo-15 catalyst (Fig. 13) in vapour phase micro-reactor. All the experiments were conducted at constant feed rate of benzene (0.4 mL/min) and air (100 mL/min). With increase in temperature, the conversion factor increased from 61 to 95%. At 663 K, the maximum conversion of benzene (95%) was attained.

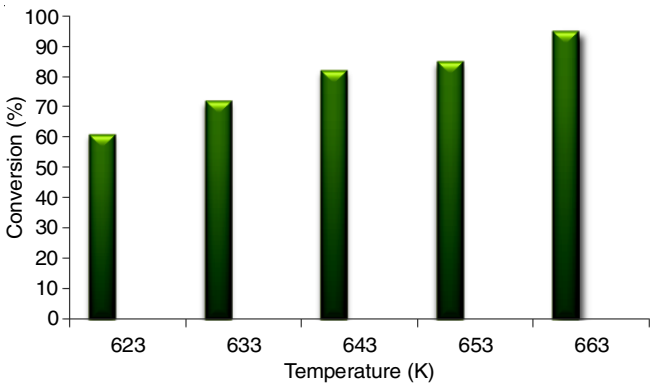

Fig. 13. Effect of temperature on conversion (%)

Effect of inlet concentration of benzene: The effect of various inlet concentration (16.03×10^{-9} to 48.10×10^{-9} mol/mL or 0.4/1.2 mL/min) on the complete oxidation of benzene at

fixed temperature (643, 653 and 663 K) have been graphically depicted as shown in Fig. 14. On increasing inlet concentration of benzene, the deep conversion decreased which illustrates that the conversion and inlet concentration varied inversely.

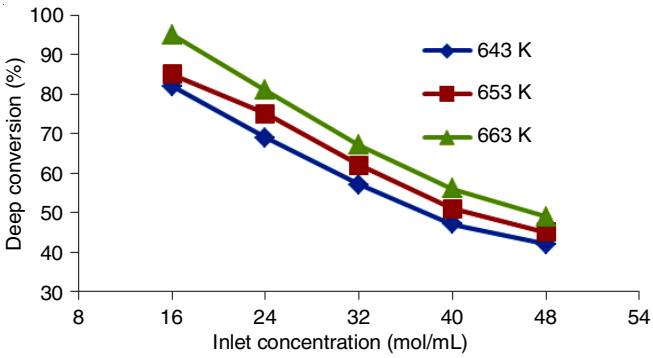

Fig. 14. Variation of deep conversion with inlet concentration of benzene

Catalyst reusability: After reaction completion, regeneration of catalyst was carried out at 673 K in presence of air. Fig. 15 shows that the results of conversion and selectivity almost remain constant upto 5th reuse cycle of catalyst, which clearly signifies that FASi/Mo-15 catalyst posses good regeneration and reusability characteristics.

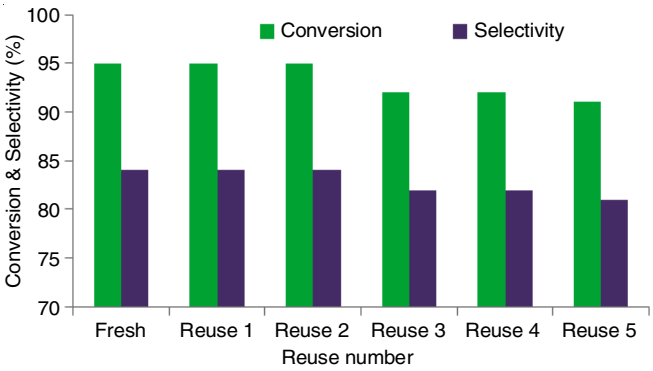

Fig. 15. Effect of catalyst reusability on conversion and selectivity

Kinetic study: Mars-van Krevelen model [55] have been implied for the kinetic study of benzene's oxidation over FASi/Mo-15 catalyst in vapour phase microreactor. According to Mars-van Krevelen model, the oxidation reaction takes place in two steps:

$$\text{Benzene} + \text{Oxidized catalyst} \xrightarrow{k_1} \text{Reduced catalyst} + \text{Products} \quad (1)$$

$$O_2 + \text{Reduced catalyst} \xrightarrow{k_2} \text{Oxidized catalyst} \quad (2)$$

The rate equation may be represented as:

$$r_1 = k_1 C_B \theta \quad (3)$$

$$r_2 = k_2 Co_2 (1-\theta) \quad (4)$$

Herein, θ is the fraction of oxidized catalyst at any time and Co_2 is concentration of oxygen.

From eqn. 3:

$$\theta = \frac{r_1}{k_1 C_B} \quad (5)$$

Putting value of θ in eqn. 4:

$$r_2 = k_2 Co_2 \left(1 - \frac{r_1}{k_1 CB}\right) \quad (6)$$

$$k_1 C_B (v_1 r_1) + k_2 Co_2 r_1 = k_1 k_2 C_B Co_2 \quad (7)$$

Therefore,

$$r_1 = \frac{k_1 k_2 C_B Co_2}{k_2 Co_2 + k_1 C_B v_1} \quad (8)$$

For a fixed bed reactor system, the integration formula of zero order and first order reaction can be expressed by following eqns. 9 and 10:

First order:

$$X = 1\text{-}\exp(-k\tau) \quad (9)$$

Zero order:

$$X = \frac{k\tau}{C_B} \quad (10)$$

Eqn. 9 indicates that for a first order reaction, the conversion (X) is unaffected by the inlet concentration of benzene (C_B) but according to eqn. 10, the conversion is inversely proportional to inlet concentration for zero order reaction.

On modifying eqns. 8-10 results in the form of eqn. 11:

$$-\ln(1-X) = -\left\{\frac{k_1 v_1}{k_2 Co_2 \times 10^6}\right\} XC_B^o + k_1 \tau \quad (11)$$

where v_1 is stoichiometric coefficient of O_2 in overall reaction (7.5), τ is average residence time (0.034 s), Co_2 is concentration of O_2, X is conversion of benzene(%), C_B^o is inlet concentration of benzene and k_1, k_2 are surface reduction rate constant and surface oxidation rate constant, respectively. The values of X, C°_B and other parameters during the reaction are given in Table-4.

The rate constant k_1 and k_2 have been calculated by plotting graphs between –ln(1-X) and XC_B^o as indicated in Fig. 16.

TABLE-4
EXPERIMENTAL RESULTS OBTAINED DURING COMPLETE OXIDATION OF BENZENE

Benzene flow rate (mL/min)	$C_B^o \times 10^{-9}$ (mol/mL)	643 K			653 K			663 K		
		X (%)	XC_B^o	-ln(1-X)	X (%)	XC_B^o	-ln(1-X)	X (%)	XC_B^o	-ln(1-X)
0.4	16.03	82	13.14	1.714	85	13.62	1.897	95	15.22	2.995
0.6	24.05	69	16.59	1.171	75	18.03	1.386	81	19.48	1.660
0.8	32.07	57	18.27	0.843	62	19.88	0.967	67	21.48	1.108
1.10	40.09	47	18.84	0.634	51	20.44	0.713	56	22.45	0.820
1.12	48.10	42	20.20	0.544	45	21.64	0.597	49	23.56	0.673

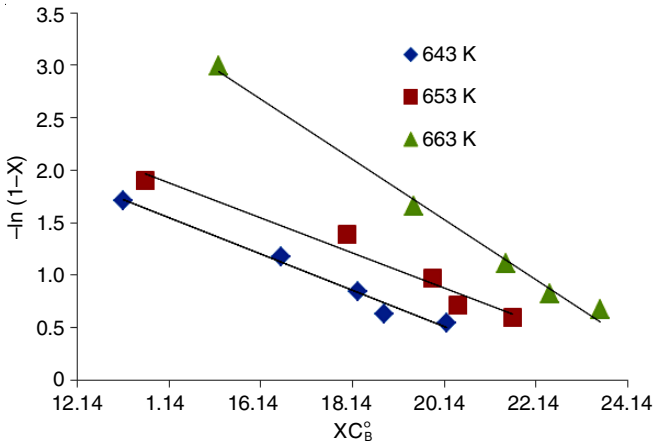

Fig. 16. Comparative linear plots at three different temperatures

The value of rate constant (k_1 and k_2) have been obtained at different temperature (643, 653 and 663 K) from the relationship between –ln(1-X) and XC°_{B} as represented in Table-5. As the temperature increases, the value of rate constant increases, which shows that rate constant is directly proportional to temperature.

TABLE-5
k_1 AND k_2 VALUES AT DIFFERENT TEMPERATURES

Temperature (K)	k_1	k_2
643	0.53×10^2	3.28×10^2
653	0.58×10^2	3.40×10^2
663	0.94×10^2	3.59×10^2

Conclusion

The present work aims at extraction of silica from different solid wastes (rice husk ash, perlite and fly ash) by using simple, rapid, low-energy, environment friendly chemical process involving alkali solubilization of the solid wastes and subsequent acid treatment. The XRD studies reveals amorphous nature of extracted silica with chief functional groups, Si-O-Si and Si-OH, which was confirmed by FT-IR too. FESEM images show agglomeration of extracted silica particles. The presence of Si and O elements and supported highly pure nature of these particles was confirmed by EDS. Surface area and ^{29}Si NMR analysis also demonstrated fine porous nature of extracted silica with excellent surface area and presence of different silanol groups and existence of silica network. Molybdenum oxide (MoO_3) was incorporated onto fly ash silica by impregnation method whose catalytic activity showed appreciable improvement with increases of Mo loading from 10 to 20 wt.%. Wherein, FASi/Mo-15 catalyst exhibits highest catalytic activity. The vapour phase oxidation reaction of benzene over catalyst follows the Mars-Van Krevelen mechanism for kinetic study, which was studied by varying temperature (623-663 K) and inlet concentration of benzene (16.03×10^{-9} to 48.10×10^{-9} mol/mL). Direct correlation was observed between deep conversion and temperature and was inversely correlated with inlet concentration. It has been deduced that the aforementioned common solid wastes may provide the raw materials necessary to produce extracted silica at industrial scale. Assuming widespread application, this strategy would help create a healthier and safer community.

ACKNOWLEDGEMENTS

One of the authors, Deepa Meena, is thankful to CSIR, New Delhi for providing the SRF fellowship. The authors also thankful to Malaviya National Institute of Technology (MNIT) Jaipur for conducting the FESEM, EDS, BET surface area analysis and SAIF, Chandigarh for FTIR and ^{29}Si NMR analysis.

CONFLICT OF INTEREST

The authors declare that there is no conflict of interests regarding the publication of this article.

REFERENCES

1. F. Ghorbani, H. Younesi, Z. Mehraban, M.S. Çelik, A.A. Ghoreyshi and M. Anbia, *J. Taiwan Inst. Chem. Eng.*, **44**, 821 (2013); https://doi.org/10.1016/j.jtice.2013.01.019
2. S. Katara, S. Kabra, D. Goyal, R. Hada, A. Sharma and A. Rani, *Mater. Today Proc.*, **42**, 1409 (2021); https://doi.org/10.1016/j.matpr.2021.01.148
3. R. Prasad and M. Pandey, *Bull. Chem. React. Eng. Catal.*, **7**, 1 (2012); https://doi.org/10.9767/bcrec.7.1.1216.1-25
4. X. Chen, E. Hadde, S. Liu and Y. Peng, *Miner. Eng.*, **113**, 41 (2017); https://doi.org/10.1016/j.mineng.2017.08.001
5. C. Contado, *Front Chem.*, **6**, 48 (2015); https://doi.org/10.3389/fchem.2015.00048
6. M. Kot, R. Wojcieszak, E. Janiszewska, M. Pietrowski and M. Zieliński, *Materials*, **14**, 968 (2021); https://doi.org/10.3390/ma14040968
7. J.A.G. Coumans, E. Demiröz, N. Kosinov and E.J.M. Hensen, *ChemCatChem*, **14**, e202200266 (2022); https://doi.org/10.1002/cctc.202200266
8. S. Faisal, P.K. Maity, Q. Zang, T.B. Samarakoon, R.L. Sourk and P.R. Hanson, *ACS Comb. Sci.*, **18**, 387 (2016); https://doi.org/10.1021/acscombsci.6b00041
9. K.R. Milleman, J.L. Milleman, J.E. Creeth, A. Butler and M.L. Bosma, *J. Clin. Dent.*, **27**, 7 (2016).
10. A. Ketov, V. Korotaev, L. Rudakova, I. Vaisman, L. Barbieri and I. Lancellotti, *Int. J. Appl. Ceram. Technol.*, **18**, 394 (2021); https://doi.org/10.1111/ijac.13654
11. P. Lu and Y.L. Hsieh, *Powder Technol.*, **225**, 149 (2012); https://doi.org/10.1016/j.powtec.2012.04.002
12. E. Phumnok, P. Khongprom and S. Ratanawilai, *ACS Omega*, **7**, 8364 (2022); https://doi.org/10.1021/acsomega.1c05848
13. A.S. Dorcheh and M.H. Abbasi, *J. Mater. Process. Technol.*, **199**, 10 (2008); https://doi.org/10.1016/j.jmatprotec.2007.10.060
14. G. Rey, S.L. Vivod, S. Singla, T. Benyo, J. King, S.S. Chuang and A. Dhinojwala, *ACS Appl. Mater. Interfaces*, **13**, 41084 (2021); https://doi.org/10.1021/acsami.1c10879
15. A. Farsad, A. Ahmadpour, T.R. Bastami and A. Yaqubzadeh, *J. Sol-Gel Sci. Technol.*, **84**, 246 (2017); https://doi.org/10.1007/s10971-017-4498-5
16. J.P. Nayak and J. Bera, *Trans. Indian Ceram. Soc.*, **68**, 91 (2009); https://doi.org/10.1080/0371750X.2009.11082163
17. X. Ma, B. Zhou, W. Gao, Y. Qu, L. Wang, Z. Wang and Y. Zhu, *Powder Technol.*, **217**, 497 (2012); https://doi.org/10.1016/j.powtec.2011.11.009
18. U. Ghani, S. Hussain, A. Ali, V. Tirth, A. Algahtani, A. Zaman, M. Mushtaq, K. Althubeiti and M. Aljohani, *ACS Omega*, **7**, 6113 (2022); https://doi.org/10.1021/acsomega.1c06553
19. H.I. El Shimi, N.K. Attia, El G.I. Diwani and El S.T. Sheltawy, *Int. J. Energy Res.*, **40**, 1743 (2016); https://doi.org/10.1002/er.3546

20. Y. Yang, P. Zhang, J. Jiang, Y. Dai, M. Wu, Y. Pan and L. Ni, *J. Sol-Gel Sci. Technol.*, **87**, 408 (2018); https://doi.org/10.1007/s10971-018-4733-8
21. M. Yoldi, E.G. Fuentes-Ordoñez, S.A. Korili and A. Gil, *Micropor. Mesopor. Mater.*, **287**, 183 (2019); https://doi.org/10.1016/j.micromeso.2019.06.009
22. M. Kasai, Y. Kobayashi, M. Togo and A. Nakahira, *Mater. Today Proc.*, **16**, 232 (2019); https://doi.org/10.1016/j.matpr.2019.05.247
23. S.K. Malpani, D. Goyal, S. Katara and A. Rani, *Chem. Pap.*, **75**, 3017 (2021); https://doi.org/10.1007/s11696-020-01501-x
24. D. Jain, C. Khatri and A. Rani, *Fuel*, **90**, 2083 (2011); https://doi.org/10.1016/j.fuel.2010.09.025
25. I. Majchrzak-Kucêba, *J. Therm. Anal. Calorim.*, **107**, 911 (2012); https://doi.org/10.1007/s10973-011-1908-8
26. J.A. Costa, V.H. Sarmento, L.P. Romão and C.M. Paranhos, *Environ. Sci. Pollut. Res. Int.*, **26**, 25476 (2019); https://doi.org/10.1007/s11356-019-05852-1
27. J.-M. Brégeault, M. Vennat, Laurent Salles, J.-Y. Piquemal, Y. Mahha, E. Briot, P.C. Bakala, A. Atlamsani and R. Thouvenot, *J. Mol. Catal. Chem.*, **250**, 177 (2006); https://doi.org/10.1016/j.molcata.2006.01.027
28. H.H. Kung, Transition Metal Oxides: Surface Chemistry and Catalysis, Elsevier (1989).
29. G. Centi, F. Cavani and F. Trifirò, Selective Oxidation by Heterogeneous Catalysis, Kluwer Academic/Plenum Publishers: New York, vol. 26 (2001).
30. A. Gervasini, L. Wahba, M.D. Finol and J.F. Lamonier, *Mater. Sci. Appl.*, **3**, 195 (2012); https://doi.org/10.4236/msa.2012.34030
31. S.V. Kotov and E. Balbolov, *J. Mol. Catal. Chem.*, **176**, 41 (2001); https://doi.org/10.1016/S1381-1169(01)00244-8
32. J.A. Melero, J. Iglesias, J.M. Arsuaga, J. Sainz-Pardo, P. De Frutos and S. Blázquez, *Appl. Catal. A Gen.*, **331**, 84 (2007); https://doi.org/10.1016/j.apcata.2007.07.031
33. Z. Song, N. Mimura, J.J. Bravo-Suárez, T. Akita, S. Tsubota and S.T. Oyama, *Appl. Catal. A Gen.*, **316**, 142 (2007); https://doi.org/10.1016/j.apcata.2006.08.029
34. F. Adam and A. Iqbal, *Micropor. Mesopor. Mater.*, **141**, 119 (2011); https://doi.org/10.1016/j.micromeso.2010.10.037
35. J. Handzlik, J. Ogonowski, J. Stoch and M. Mikolajczyk, *Catal. Lett.*, **101**, 65 (2005); https://doi.org/10.1007/s10562-005-3751-7
36. R.S. Medeiros, J.G. Eon and L.G. Appel, *Catal. Lett.*, **69**, 79 (2000); https://doi.org/10.1023/A:1019093116966
37. A. Christodoulakis, E. Heracleous, A. Lemonidou and S. Boghosian, *J. Catal.*, **242**, 16 (2006); https://doi.org/10.1016/j.jcat.2006.05.024
38. M. Mathew, A.V. Biradar, S.B. Umbarkar and M.K. Dongare, *Catal. Commun.*, **7**, 394 (2006); https://doi.org/10.1016/j.catcom.2005.12.022
39. F.F. Oloye and I.A. Ololade, *Chemistry Africa*, **1**, 119 (2018); https://doi.org/10.1007/s42250-018-0016-6
40. K. Jiratova, A. Spojakina, J. Balabanova, R. Palcheva, G. Tyuliev and Y. Karakirova, *React. Kinet. Mech. Catal.*, **125**, 901 (2018); https://doi.org/10.1007/s11144-018-1462-5
41. K.C. Pratt, J.V. Sanders and V. Christov, *J. Catal.*, **124**, 416 (1990); https://doi.org/10.1016/0021-9517(90)90189-Q
42. D. Hamon, M. Vrinat, M. Breysse, B. Durand, M. Jebrouni, M. Roubin, P. Magnoux and T. des Courières, *Catal. Today*, **10**, 613 (1991); https://doi.org/10.1016/0920-5861(91)80042-8
43. P. Topka, H. Balcar, J. Rathouský, N. •ilková, F. Verpoort and J. Èejka, *Micropor. Mesopor. Mater.*, **96**, 44 (2006); https://doi.org/10.1016/j.micromeso.2006.06.016
44. J. Li, J. Liu, L. Ren, Q. Liu, Z. Zhao, Y. Chen, P. Zhu, Y. Wei, A. Duan and G. Jiang, *J. Energy Chem.*, **23**, 609 (2014); https://doi.org/10.1016/S2095-4956(14)60191-1
45. J.A. Bergwerff, T. Visser, G. Leliveld, B.D. Rossenaar, K.P. de Jong and B.M. Weckhuysen, *J. Am. Chem. Soc.*, **126**, 14548 (2004); https://doi.org/10.1021/ja040107c
46. S. Alehyen, M.E. Achouri and M. Taibi, *J. Mater. Environ. Sci.*, **8**, 1783 (2017).
47. P.P. Nayak and A.K. Datta, *Silicon*, **13**, 1209 (2021); https://doi.org/10.1007/s12633-020-00509-y
48. Z.A. Supardi, Z. Nisa, D.H. Kusumawati, N.P. Putri, A. Taufiq and N. Hidayat, *J. Phys: Conf. Ser.*, **1093**, 012025 (2018); https://doi.org/10.1088/1755-1315/276/1/012046
49. Munasir, Triwikantoro, M. Zainuri and Darminto, *Mater. Sci. Pol.*, **33**, 47 (2015); https://doi.org/10.1515/msp-2015-0008
50. E.A. Paukshtis, M.A. Yaranova, I.S. Batueva and B.S. Bal'zhinimaev, *Micropor. Mesopor. Mater.*, **288**, 109582 (2019); https://doi.org/10.1016/j.micromeso.2019.109582
51. V.K. Yadav and M.H. Fulekar, *Mater. Today Proc.*, **18**, 4351 (2019); https://doi.org/10.1016/j.matpr.2019.07.395
52. G. Engelhardt and H. Jancke, *Polym. Bull.*, **5**, 577 (1981); https://doi.org/10.1007/BF00255295
53. A. Kido, H. Iwamoto, N. Azuma and A. Ueno, *Catal. Surv. Asia*, **6**, 45 (2002); https://doi.org/10.1023/A:1020541200687
54. A.V. Biradar, S.B. Umbarkar and M.K. Dongare, *Appl. Catal. A Gen.*, **285**, 190 (2005); https://doi.org/10.1016/j.apcata.2005.02.028
55. S.B. Lee, S.L. Kang, J.D. Lee and I.K. Hong, *J. Ind. Eng. Chem.*, **5**, 170 (1999).